






RESEARCH ARTICLE | FEBRUARY 06 2025

Large volume torsion (LVT) apparatuses for rock deformation at high pressure and temperature

Philip Skemer ; Hélène Couvy ; Andrew J. Cross ; Joshua A. H. Littleton ; Caroline Bollinger 



Rev. Sci. Instrum. 96, 023903 (2025)

<https://doi.org/10.1063/5.0221218>



Articles You May Be Interested In

An apparatus for measuring nonlinear viscoelasticity of minerals at high temperature

Rev. Sci. Instrum. (July 2021)

Simultaneous generation of ultrahigh pressure and temperature to 50 GPa and 3300 K in multi-anvil apparatus

Rev. Sci. Instrum. (October 2021)

In situ measurements of electrical resistivity of metals in a cubic multi-anvil apparatus by van der Pauw method

Rev. Sci. Instrum. (May 2022)



Special Topics Open for Submissions

[Learn More](#)

Large volume torsion (LVT) apparatuses for rock deformation at high pressure and temperature

Cite as: *Rev. Sci. Instrum.* **96**, 023903 (2025); doi: [10.1063/5.0221218](https://doi.org/10.1063/5.0221218)
Submitted: 30 May 2024 • Accepted: 19 January 2025 •
Published Online: 6 February 2025



View Online



Export Citation



CrossMark

Philip Skemer,^{1,a)}  H el ene Couvy,¹  Andrew J. Cross,²  Joshua A. H. Littleton,³ 
and Caroline Bollinger¹ 

AFFILIATIONS

¹Department of Earth, Environmental, and Planetary Sciences, Washington University in St. Louis, St. Louis, Missouri 63130, USA

²Department of Geology and Geophysics, Woods Hole Oceanographic Institution, Falmouth, Massachusetts 02543, USA

³Department of Materials, University of Manchester, Manchester, England M13 9PL, United Kingdom

^{a)}Author to whom correspondence should be addressed: pskemer@wustl.edu

ABSTRACT

Laboratory studies of rock rheology rely on purpose-built devices that can apply planetarily relevant pressures, temperatures, and non-hydrostatic stresses. Generating these pressures and stresses requires the application of large forces over small specimen areas. However, because rocks are generally polymineralic and deformation microstructures form across many length scales, it is advantageous to study relatively large (millimetric) specimens. In addition, many microstructures continue to evolve with progressive strain, so it is vital that some apparatus are able to generate enough shear strain to study these deformation phenomena. This contribution describes two new rock deformation apparatus—the Large Volume Torsion apparatus—at Washington University in St. Louis, which are capable of deforming geological specimens at high pressure and temperature ($P = 3$ GPa; $T = 1800$ K). Deformation is imposed in a torsional geometry, which enables the generation of extremely large shear strains ($\gamma > 100$) relevant to Earth's plate boundaries and convecting mantle. A large specimen (diameter up to 4.2 mm) permits detailed postmortem microstructural analysis. Apparatus design, calibration, experimental procedures, and some examples of applications are reviewed.

Published under an exclusive license by AIP Publishing. <https://doi.org/10.1063/5.0221218>

I. INTRODUCTION

The interiors of rocky planets are dynamic environments where primordial and radiogenic heat may be transmitted to the surface by solid-state convection. On Earth, mantle convection is the driving force for plate tectonics and all of its accompanying geological phenomena.^{1,2} On other terrestrial planets, such as Venus, convection is thought to occur beneath a largely stable “stagnant” lithosphere.³ The characteristics and vigor of mantle convection, and the style of surface tectonics, are largely determined by the rheological properties of the rocks that comprise the planetary interior.⁴

Although Earth is almost entirely solid from the surface to the core–mantle boundary, rocks behave like a fluid over geological time-scales at depths below ~ 15 km where the pressure ($P > 0.5$ GPa) and temperature ($T > 800$ K) promote viscous flow

while suppressing brittle fracture.⁵ Unfortunately, rocks at these depths are inaccessible to direct observation, a problem only exacerbated when considering the interiors of neighboring planets and distant exoplanets. Moreover, planetary deformation takes place across vast eons of geologic time, complicating its study on human time-scales. Therefore, the study of planetary interiors depends crucially on laboratory methods that can determine the material properties of rocks by reproducing extreme temperature, pressure, stress, and strain conditions. This paper describes a pair of devices called Large Volume Torsion (LVT) apparatus, which are designed to conduct experiments on the microstructural and rheological evolution of rocks at conditions relevant to the interior of Earth, other rocky planets, and moons. The LVTs (henceforth LVT1 and LVT2) were built in 2013 and 2020, respectively, in the Rock Deformation Lab of the Department of Earth, Environmental, and Planetary

Sciences at Washington University in St. Louis. Both LVTs are solid-medium apparatus based conceptually on the Rotational Drickamer Apparatus.⁶ The LVTs use conical “Drickamer-style” anvils⁷ to generate pressure and a cylindrical internal heating element to produce temperature conditions relevant to Earth’s upper mantle ($P = 3$ GPa; $T = 1800$ K). In addition, a torsional actuator rotates one of the anvils, allowing the LVTs to generate enormous shear strains ($\gamma > 100$) over a wide range of strain rates on cylindrical specimens that are 4.2 mm in diameter.

II. BACKGROUND

Many apparatuses have been designed to deform rocks in a laboratory setting, dating back to the late nineteenth century.^{8,9} However, development accelerated in the second half of the 20th century due to a burgeoning interest in the physics of plate tectonics and mountain building.^{10,11} In the scientific study of rock mechanics, experimental apparatus are selected for their ability to access a certain range of deformation conditions, which may include pressure, temperature, displacement rate, pore-fluid pressure, and so on. The specific attributes of each apparatus reflect the scientific questions that it is intended to address.

A rock deformation apparatus used at confining pressure greater than 1 atm must apply that pressure to the specimen through some type of fluid medium,¹¹ which may be a gas, liquid, or low viscosity solid. Solid-medium apparatus, such as the LVT described in the present work, the Rotational Drickamer Apparatus⁶ (RDA), the Deformation-DIA¹² (D-DIA), or the eponymous Griggs Apparatus,¹³ are able to generate the greatest confining pressures. However, solid media also exert considerable friction when in contact with moving deformation pistons, which compromises external stress measurements.^{14,15} In contrast, liquid or gas-medium devices such as a Heard-type¹⁶ or Paterson-type apparatus¹⁷ are able to resolve stress with far greater accuracy using load cells that sit inside the pressure vessel, but are typically limited to lower confining pressures ($P_{\max} < 0.5$ GPa). As such, solid-medium apparatus are chosen when it is necessary or advantageous to conduct experiments at greater confining pressure.

Among the varied designs for solid-medium apparatus, there are three basic geometries with which strain can be imposed: axial, direct shear, and torsion. Axial geometries compress cylindrical specimens parallel to the axis of the cylinder and are effectively limited to maximum shortening strains of about $\epsilon \sim 0.5$. In a direct shear configuration, a thin sample is sheared between two hard pistons saw-cut at 45° to the axis of compression. Direct shear experiments are generally limited to shear strains of $\gamma \sim 3$, although some exceptional experiments have been achieved.¹⁸ In torsional configurations, samples are sheared between two parallel rotating plates, and there is no geometric limit to the amount of shear strain that can be imposed.^{19,20} Torsional apparatus are chosen when it is necessary to conduct experiments to large strains. The only apparatus capable of deforming rocks in torsion at high pressure ($P > 1$ GPa) and temperature are the LVT, RDA,⁶ rotational Paris-Edinburgh (PE) cell,^{21,22} and rotational diamond anvil cells (rDAC).^{23–26} Of these, the LVT is able to achieve the greatest strains due in part to its stability over experimental durations of days to weeks. LVT specimens (typically 4.2 mm in diameter) are also the largest among this set of apparatus: PE cells are slightly smaller at 3.5 mm in diameter, RDA

specimens are 1.2 mm in diameter, and rDAC specimens may be only $50 \mu\text{m}$ in diameter (although in all cases larger sample dimensions are technically feasible). Large specimens (i.e., with dimensions that are a factor of 10^2 – 10^4 greater than the grain size) are critical for microstructural studies because of the varied length scales over which deformation microstructures develop.²⁷ A large volume of measurable material is necessary for statistically meaningful analyses.²⁸

III. LARGE VOLUME TORSION APPARATUS DESCRIPTION

Figure 1 shows the two LVT apparatus and a composite schematic. In the LVT1, force to generate confining pressure (up to ~ 3 GPa) is applied with a 100 ton hydraulic cylinder mounted to an Enerpac press frame. The total weight of the press frame is ~ 2000 kg.

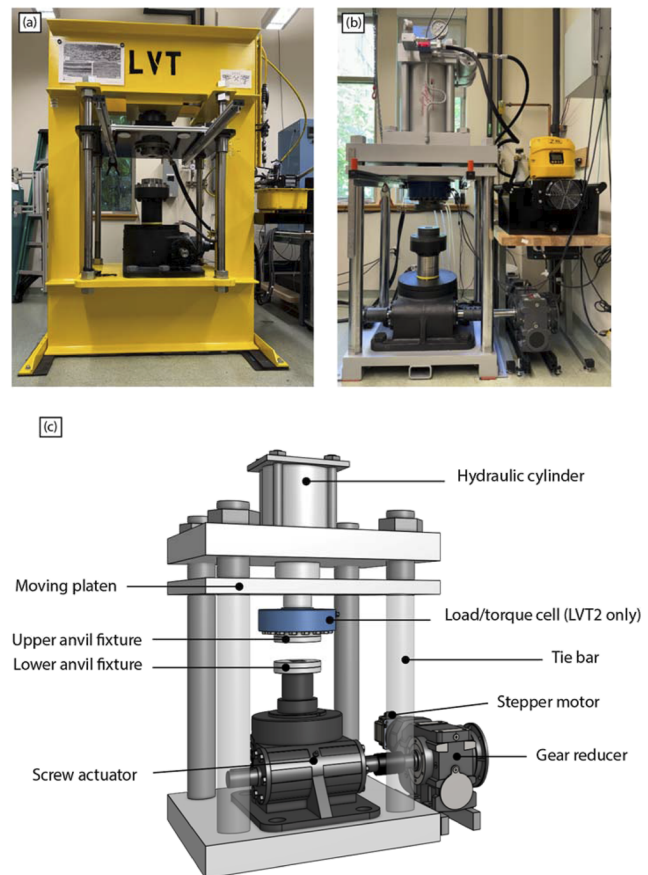


FIG. 1. Large Volume Torsion (LVT) apparatus are used for high pressure and temperature deformation of rock specimens. (a) LVT1 constructed in 2013. (b) LVT2 constructed in 2020. (c) Composite schematic diagram of the LVT apparatus, showing some key components. Anvils that drive deformation sit between the upper and lower anvil fixtures (see Fig. 2). The upper anvil is fixed to the loading frame, while the lower anvil is rotated using a screw actuator powered by a small stepper motor.

The hydraulic cylinder is actuated by a double-acting hand pump. Oil pressure is monitored with an analog gauge and a digital pressure transducer (Omega), and the pressure is confined in a water-cooled, strip-wound pressure vessel with a tungsten carbide core and an inner diameter of 40 mm (Strecon A/S) (Fig. 2). Force is applied to tungsten carbide Drickamer-style anvils with a 20° taper (Kennametal CD-630, fabricated by Dura-Metal) that fit in the bore of the pressure vessel. The circular cullet surfaces (6.35 mm diameter) of the anvils are laser engraved in a grid or fin-like pattern to strengthen the mechanical coupling between the sample and anvils.

Specimens are internally heated to temperatures of up to 1800 K using a cylindrical graphite heater surrounding the sample (Fig. 3). Thermocouples may be used to measure temperature and calibrate the temperature-power relationship during static experiments (See Sec. V B). Power to the heater is supplied by a single-phase 3 kVA power supply (Deltech, Inc.) via a pair of 4/0 welding cables. The power supply cabinet includes a 205 VAC to 6 VAC step-down transformer that can generate up to 300 A current. A Eurotherm (model 3504) temperature controller is used to adjust the output.

Shear is induced by rotating one anvil with respect to the other. The upper anvil is anchored to the press frame while the lower anvil is rotated using a screw actuator (Simplex/UniLift) with an integrated worm gear that translates rotation about a horizontal axis to rotation about a vertical axis (gear ratio 36:1). A thrust bearing assembly within the screw actuator, which is rated to 100 tons, minimizes the torque required to induce rotation under high normal stresses. A microstepper motor with a planetary gearhead, both from Applied Motion Products (gear ratio 4:1) and a five-stage helical bevel gear reducer from Hub City (gear ratio 3352:1), are coupled to the screw actuator to drive rotation. The total gear ratio (482 688:1) allows the apparatus to access a wide range of shear strain rates, from 5×10^{-8} to $1 \times 10^{-3} \text{ s}^{-1}$ for a specimen of the chosen dimensions. These experimental strain rates are necessarily faster than tectonic

strain rates, which are on the order of 1×10^{-13} to $1 \times 10^{-15} \text{ s}^{-1}$. A torque sensor that also measures rotational displacement (Interface) is coupled between the UniLift screw actuator and Hub City gear reducer.

Communication with the instrument, enabling external and remote control of the temperature and rotation rate and the collection of process data (pressure, voltage, current, rotation angle, and torque), is achieved using multiple sensors and a digital acquisition system (CompactDAQ) from National Instruments. LabView software is used for data acquisition and control.

The LVT2 maintains very similar design specifications to the LVT1 but with a few modifications. LVT2's press frame, which has a four-post design, is rated to 150 tons. The axial load is applied by a double-acting hydraulic cylinder custom-built by Milwaukee Cylinder. Axial loads are both measured and controlled using a dual-axis load/torque cell (Interface) and actuated by a servo valve (Moog) that is electronically controlled by a Delta Computer System and RMC software. The load/torque cell is placed between the hydraulic cylinder and the top anvil fixture for measurement accuracy. Oil pressure is produced by an electric Enerpac pump and stabilized using a nitrogen-charged pressure accumulator (Milwaukee Cylinder). The rotation angle is measured using a rotary encoder (Red Lion Controls).

IV. INTERNAL CELL ASSEMBLY

A. Cell assembly design

Figures 3(a) and 3(b) show the two different “cell assembly” designs developed for torsion experiments. Figure 3(c) is a photograph of machined parts prepared for an experiment. The term cell assembly refers to the metal and ceramic parts that are used to transmit loads from the apparatus to the experimental specimen and to provide an electrical path through the internal heating element (the

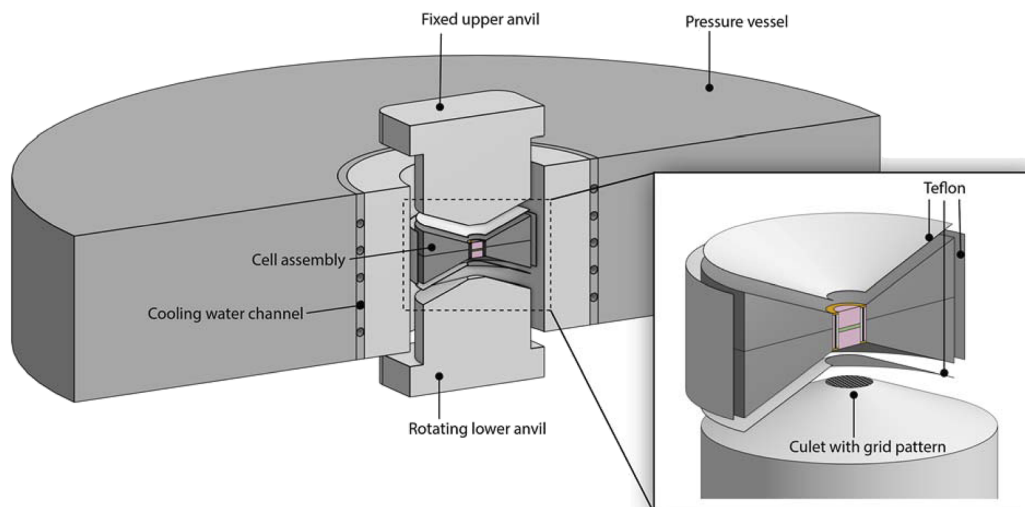


FIG. 2. Exploded cut-away schematic diagram illustrating the pressure vessel, anvils, and cell assembly.

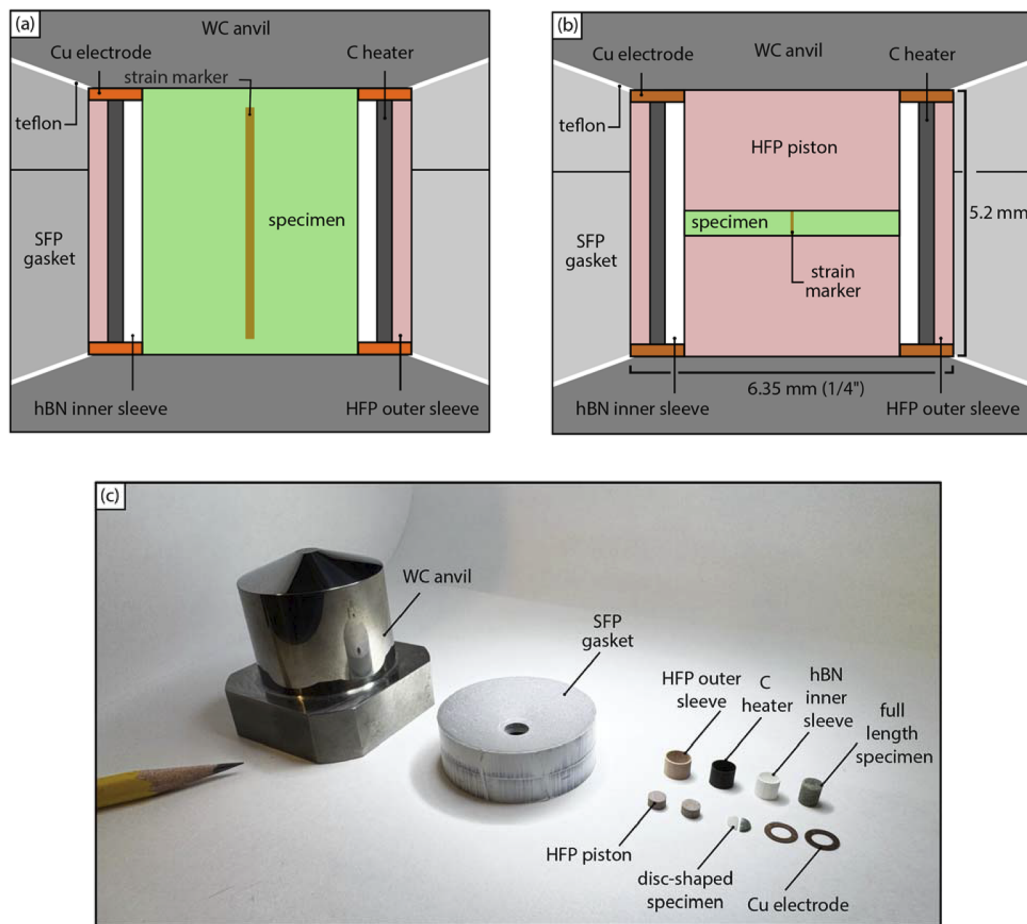


FIG. 3. Schematic cross section of the torsion cell assemblies: (a) full-length specimen and (b) disk-shaped specimen (not to scale). WC = tungsten carbide; SFP = soft-fired pyrophyllite; HFP = hard-fired pyrophyllite; Cu = copper; C = graphite; hBN = hexagonal boron nitride. (c) Various components ready for final assembly.

“heater”). All components of the cell assembly sit inside the pressure vessel (Fig. 2). The dimensions of all the parts are similar for both designs. The nature of the specimen and the experimental objectives dictate which design is the most appropriate.

The outermost part of the cell assembly is a pair of conical gaskets made of soft-fired pyrophyllite. The gaskets are made of soft-fired pyrophyllite and act as the pressure medium, providing lateral support to the heater while converting the axial forces to hydrostatic pressure in the experimental specimen itself. The 20° angle of the gasket is beveled to 19° at a distance of 3 mm from the outer edge to allow for some compaction of the assembly. This assembly compaction helps ensure that there is reliable electrical contact between the anvil and the cell assembly during the loading process. The two halves of the gasket have different thicknesses (i.e., their joining surface is vertically offset from the center of the assembly) to minimize the propagation of unwanted tensile cracks through the sample when unloading an experiment. The pair of gaskets is wrapped in Teflon tape to hold them together while assembling and loading into the pressure vessel, and to facilitate the

extraction of the cell assembly from the pressure vessel at the end of an experiment. The specimen is heated by running a current through a graphite sleeve that has a wall thickness of $200\ \mu\text{m}$ and can routinely reach 1800 K. $250\ \mu\text{m}$ thick copper electrodes are placed at the top and bottom of the heater, in contact with the anvils, to ensure a good electrical connection. Kapton film is wrapped around one of the anvils to keep the heater from short-circuiting through the pressure vessel. The heater is supported by a hard-fired pyrophyllite outer sleeve and isolated from the sample by an inner sleeve made of either soft-fired pyrophyllite or hexagonal boron nitride (hBN). hBN is preferred due to its high melting temperature, low strength, and low reactivity with geological materials of interest. However, some weaker samples require extra lateral support to avoid extrusion during initial loading, and for these materials, soft-fired pyrophyllite is used in place of hBN. If the nature of the material allows it, a full-length specimen in direct contact with both anvils is placed in the inner sleeve [Fig. 3(a)], maximizing the frictional coupling between the specimen and the anvils. If specimen coring is not possible, two hard-fired pyrophyllite pistons are used to sandwich a disk-shaped

sample [Fig. 3(b)]. A drawback of this design is that the two additional interfaces within the cell assembly may slip during torsional deformation. To measure the strain applied to the specimen post-mortem, an initially vertical passive strain marker is placed within the sample, bisecting the two halves of the sample cylinder. The strain marker is typically a weak metal, made of either a layer of sputter-coated gold or a thin foil of nickel.

B. Fabrication

The cell assembly is fabricated for each experiment and is not reusable. To ensure reproducibility among each experimental run, all parts of the assembly except the copper electrodes are fabricated in-house using a Roland MDX-40A milling machine equipped with solid carbide tooling. A model of each part is created using SketchUp software. For practicality, large sheets of raw material (graphite, soft-fired pyrophyllite, or hBN) with the appropriate thickness are attached to the milling machine working table using removable CrystalBond epoxy. Each part is milled from the top down, and several parts can be made at the same time.

Raw materials are procured from various vendors and are either used as-is or transformed to modify physical properties. Pyrophyllite sheets (preferably Grade “A” from Maryland Lava) are soft-fired at 1123 K for various durations depending on their thickness (3 h for the outer sleeves and the pistons and 10 h for the gaskets). Ultra-fine-grained graphite sheets are procured from Bar-Lo (Grade B325). Different graphite grades such as UPF4 from Mersen or EDM-4 from POCO Graphite were tested without consistent success. The hBN sheets are HBC grade (the highest purity hot-pressed BN grade) from Momentive Performance Material.

The sleeves of the assembly (inner, outer sleeve, and heater) have a minimum concentricity of 90% and a thickness tolerance of $\pm 10 \mu\text{m}$. After milling, only a light sanding is necessary to adjust the height. Pyrophyllite pistons and outer sleeves are hard-fired at 1373 K for 30 min after fabrication.

Copper electrodes are manufactured locally by Gateway Laser Services, St Louis, MO, using a laser micromachining technique. The inner diameter of the electrodes is intentionally undersized to be adjusted individually to the correct specimen/piston diameter.

C. Specimen preparation

The preparation of specimens varies according to the scientific goals and the choice of assembly design. The most efficient way to prepare and shear a specimen is to core a sample from a single crystal or polycrystalline rock. The specimens are then fully dense, typically chemically equilibrated, and provide a solid surface to grip the anvils. Cores are drilled using a bench-top drill press and a water-cooled diamond coring bit. The diameter of the extracted cores is nominally 4.2 and ~ 5 mm long, but can vary slightly depending on the specimen material and the wear of the coring bit itself. In the case of friable specimens or when the use of synthetic specimens is necessary, powders are cold-pressed in a hydraulic press using a 4.2 mm diameter pellet die. The pellet density is close to 70% of its theoretical maximum (i.e., $\sim 30\%$ remnant porosity). The pellet height is typically only 0.5–0.8 mm to minimize excessive shortening of the cell assembly during the experimental loading phase, which can cause the heater to fail.

V. CALIBRATIONS

The torsional geometry of the LVTs limits direct access to the cell assembly that would permit routine thermocouple measurements of specimen temperature during deformation. Therefore, a series of static pressure and temperature calibrations were performed to (1) calibrate the relationships between load and pressure and (2) calibrate the relationship between power output to the heating element and sample temperature. These calibration experiments were conducted iteratively to establish dimensions of the cell height, resistance heater thickness, and gasket profile that provide optimal pressure efficiency while minimizing the axial and radial temperature gradients.

A. Pressure calibration

Pressure within the cell assembly was calibrated against the axial force applied by the hydraulic cylinder. The relationship between hydrostatic pressure on the specimen itself and applied force is assumed to be linear, but the calibration cannot be easily determined *a priori* due to the anvils' conical shape and the spacing between the culets. For both LVT apparatuses, the calibration was performed using the bismuth I–II phase transition, which is detected by a drastic reduction in electrical resistivity at 2.55 GPa and room temperature.^{29,30} As shown in Fig. 4(a), copper electrical leads were connected to a thin strip of bismuth in the center of the assembly. Under load, the tungsten carbide anvils are in contact with the copper leads on both sides of the pressure cell, which closes the circuit. An ohmmeter was connected to the upper and lower anvils to continuously measure the electrical resistance through the circuit while incrementally increasing the applied force. The resistance was monitored until a large reduction was observed over a small range of increasing applied force, which indicates that the bismuth I–II transition has occurred. The force applied at the point of the transition is the force required to generate 2.55 GPa of confining pressure. A linear fit between applied force and pressure is a reliable means to estimate confining pressure on the specimen up to a limit of ~ 3 GPa.

The pressure determined by this method represents a maximum value. However, there is a radial gradient in pressure from the center of the assembly toward the gasket. A minimum pressure, within the gasket, can be estimated from the axial load applied by the hydraulic ram divided by the cross-sectional area of the anvil. At peak load—100 tons for LVT1 and 150 tons for LVT2—this minimum pressure is 0.7 and 1.1 GPa, respectively. Typically, we assume a linear gradient where the pressure in the center of the assembly is assumed to equal the value calibrated using the bismuth phase transition, and the pressure at the edge of the culet is assumed to be the minimum pressure.

B. Temperature calibration

The use of a thermocouple during a torsional deformation experiment is unreliable because the leads may be sheared off or the wires may inadvertently create a short circuit through the cell assembly. In addition, the alumina sheaths that are used to provide electrical insulation around thermocouples may introduce mechanical instabilities or other sources of experimental error. However, static experiments (i.e., experiments in which no deformation is

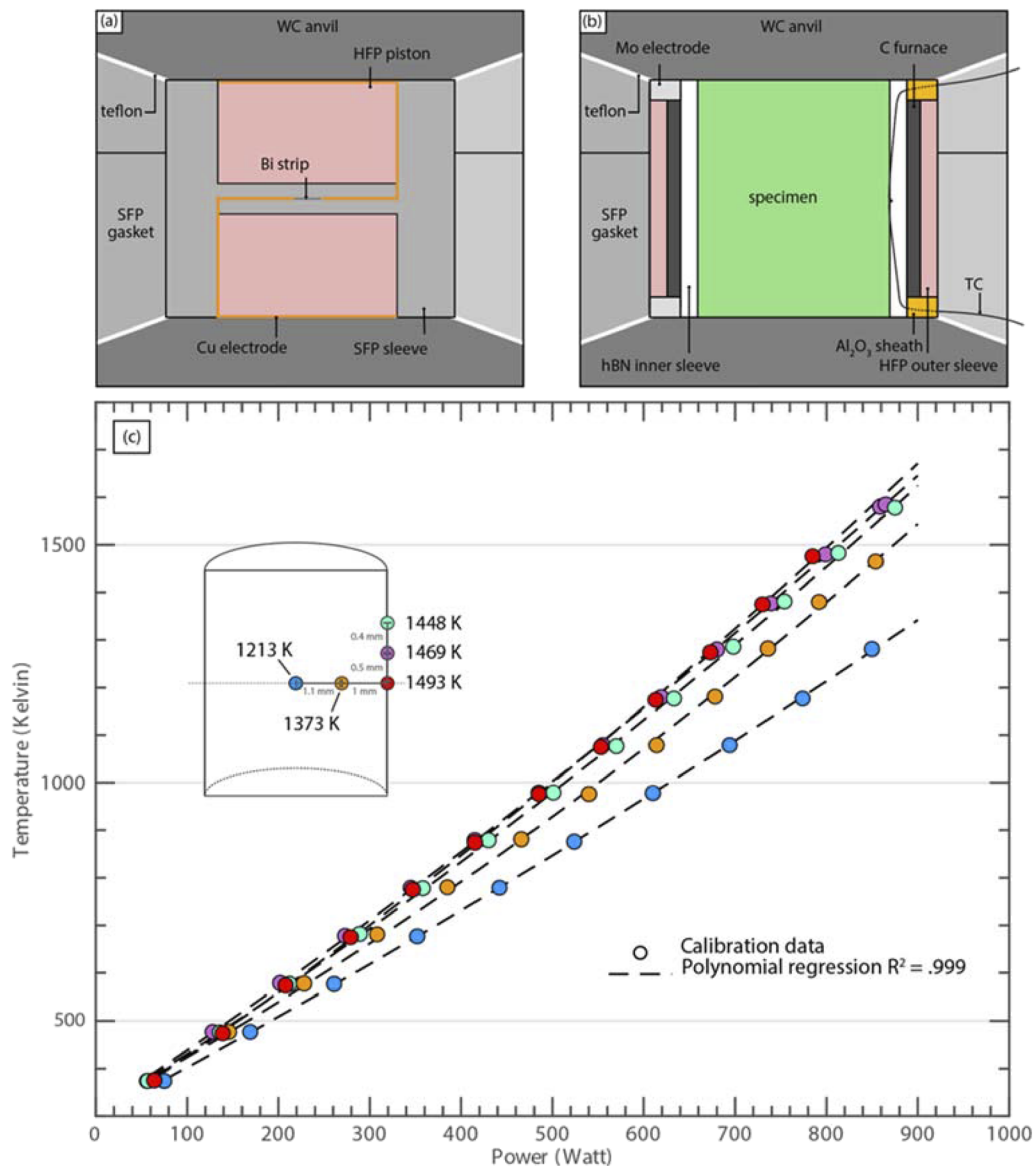


FIG. 4. Schematic cross-section of (a) a pressure calibration cell assembly and (b) a temperature calibration cell assembly (not to scale). WC, tungsten carbide; SFP, soft-fired pyrophyllite; HFP, hard-fired pyrophyllite; Cu, copper; Mo, molybdenum; Bi, bismuth; C, graphite; hBN, hexagonal boron nitride; Al₂O₃, aluminum oxide; TC, Type-R thermocouple. (c) The relationship between power (Watts) and temperature (K) for each thermocouple junction position. The inset represents a specimen cross-section with thermocouple junction positions and temperatures measured under the same power condition (800 W).

imposed) can be used to calibrate a relationship between the power applied to the heating element and the temperature at various positions within the cell assembly. These calibrations are reproducible and can be used to ensure consistent deformation conditions from experiment to experiment, even if there is some uncertainty in the absolute accuracy of the temperature estimate.³¹ Temperature calibration experiments were conducted using the cell assembly shown in Fig. 4(b). A Type-R thermocouple (87% Pt/13% Rh – 100% Pt) is first placed at the perimeter of an Åheim dunite specimen with

the thermocouple junction placed at half the assembly height, which is the hottest part of the heater. The temperature read at this position is defined as the specimen temperature (since for torsion tests, we are interested in the microstructures formed at the outer edge of the specimen where strain is greatest). We do not correct for the pressure effect on the thermocouple reading, which is minimal at these conditions. The wires passing over the resistance heater are insulated by small alumina sheaths, one on each side of the heater. The copper electrodes are replaced by thicker

molybdenum electrodes (500 μm thick) to protect the alumina sheaths from being crushed during compression. The total cell assembly is slightly taller—6.2 mm instead of 5.2 mm for a standard deformation assembly—but the graphite heater's dimensions are the same as the one used in the standard torsion cell. To establish the temperature profile of the sample, several experiments were conducted at the same load (80 tons of force) and with five different thermocouple junction positions, covering the sample region of interest. The calibration results are presented in Fig. 4(c). The temperature data are fit using a second-order polynomial regression equation ($R^2 = 0.999$). In the radial plane, temperature decreases markedly with distance from the heater (~ 120 K/mm near the sample edge). There is also an axial thermal gradient, but this is comparatively small (~ 50 K/mm).

VI. INSTRUMENT OPERATION

A. Performing an experiment

Most experiments follow a standard loading and heating path that has been determined to maximize the longevity of the graphite heater, which is the primary limitation to the duration of experiments. Once the pressure vessel is loaded with the cell assembly, it is placed on top of the lower anvil. The press is then closed by lowering the top anvil into the pressure vessel before the hydraulic ram is pressurized slowly until it is applying ~ 10 tons of force. This force closes all of the gaps in the ceramic assembly and creates good contact between the anvils, electrodes, and the heater. Temperature and pressure are then incrementally increased along a given pressure-temperature path until the desired run conditions are reached. The process takes about two hours. The cell assembly then sits statically for approximately one hour to equilibrate and relax any unwanted non-hydrostatic stresses generated during compression. To begin the dynamic portion of the experiment, the stepper motor is set to a specific rotation speed corresponding to a desired strain rate. All LVT specimens are sheared dextrally by convention, but it is trivial to conduct equivalent experiments with a sinistral shear sense. The duration of an experiment varies from hours to up to two weeks, depending on the required shear strain and strain rate. Once the target strain is reached, the motor is stopped and the specimen quenched immediately by turning off the graphite heater's power supply. Decompression is achieved by slowly releasing the hydraulic cylinder oil through a series of adjustable flow valves. Once room pressure is reached, the cell assembly is extracted from the pressure vessel and prepared for postmortem analysis.

B. Postmortem analysis

At the conclusion of an experiment, the anvils are removed and the cell assembly is extracted from the pressure vessel using the hydraulic cylinder. The exposed surfaces of the specimen or forcing pistons are photographed and checked for any indication of slip, which would indicate an unsuccessful experiment. Then, the whole cell assembly is embedded in epoxy to protect the specimen from fragmenting along potential decompression cracks. Once the epoxy has cured, the specimen is cut tangentially to the cylindrical specimen, close to its perimeter, and polished to allow observation under an optical microscope. The tangent cut is made in such a way as to also view the strain marker. The rotation angle of the strain marker

from its original vertical position quantifies the strain undergone by the specimen (see Paterson and Olgaard, 2000 for details on this calculation). The polished section produced can be used for further analyses using a scanning electron microscope (SEM) with electron backscatter diffraction (EBSD) or a transmitted electron microscope (TEM) to investigate the development of deformation microstructures. The specimen can also be mounted on glass and polished to the standard thickness for petrographic light microscopy (30 μm). Due to the large specimen size, more than one thin or thick section can be produced.

VII. EXPERIMENTAL RESULTS

In this section, we highlight some experimental results from studies conducted using LVT apparatus. By virtue of its ability to achieve large strains on geologic specimens in a viscous or crystal plastic deformation regime, the LVTs are well-suited for studies of microstructural evolution. The relatively capacious sample volume also facilitates the exploration of microstructures across a range of scales. Both research thrusts described in this section leverage the unique capabilities of the LVT apparatus.

A. Generation of mylonites

Mylonites are fine-grained rocks that are ubiquitous features of boundaries between tectonic plates and are interpreted to represent the product of localized deformation at high pressure and temperature.^{32–34} There are two features of mylonites that distinguish them from typical host rocks: grain sizes that may be reduced by orders of magnitude, and mineral phases that are generally well-mixed.^{35,36} Together, these microstructural characteristics are thought to promote localized weakening of the lithosphere over long geologic intervals, an essential feature of Earth-like plate tectonics.^{37,38}

Experiments on composites of two or more minerals seek to clarify how different mineral phases mix together at relevant deformation conditions. Across several studies using the LVT apparatus, numerous mineral compositions have been tested to examine the role of viscosity contrast, varying phase proportions, and differing degrees of chemical stability.^{28,39–41}

Experiments up to shear strains of $\gamma > 100$ show several trends, some of which can be seen in SEM images (Fig. 5). With increasing shear strain, the spatial density of phase boundaries (quantified as the total length of boundaries between dissimilar minerals per unit area) increases. Meanwhile, the thickness of monomineralic domains decreases as they are stretched and thinned.²⁸ Grain size is reduced, in some cases well below the grain size predicted by single-phase grain-size piezometers. Roughness along the phase boundary interface arises from the formation of interphase triple junctions.³⁹ Some mixing occurs by grain switching/migration across these interfaces; however, most mixing (among chemically dissimilar minerals) appears to result from the geometric thinning and necking of monomineralic domains. This “geometric mixing” yields a scaling relationship that can be used to determine the critical strains required for the obliteration of compositional layering and thus the formation of ultramylonites. The strains required to achieve microstructural and rheologic steady state are now understood to depend on several factors, including the initial phase domain size

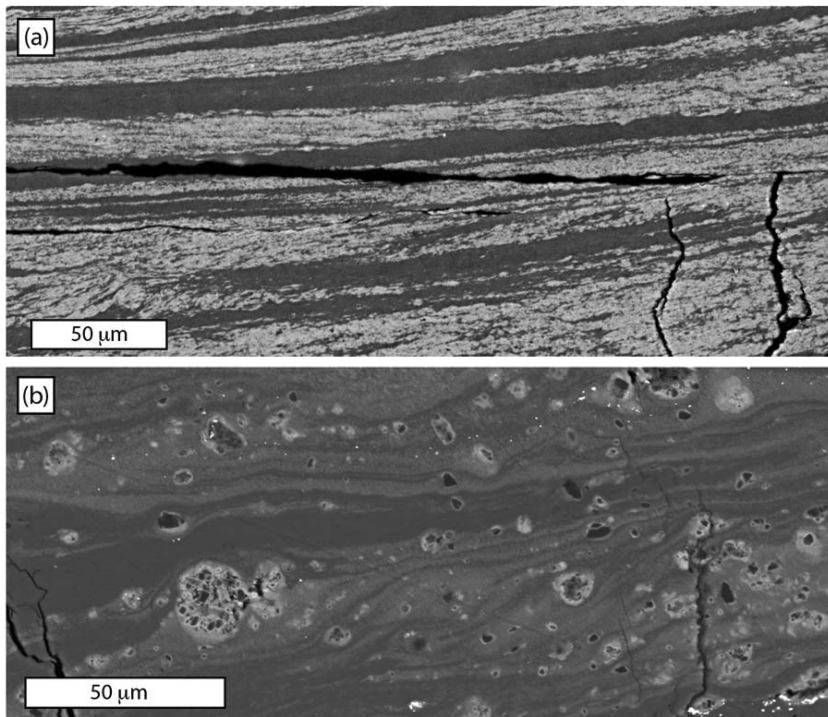


FIG. 5. Backscatter electron (BSE) images of two experiments on highly deformed multi-component geologic systems. (a) Experiment LVT_115 was conducted on a 50/50 vol. % mixture of the minerals calcite (darker gray) and anhydrite (lighter gray), both of which are fully plastic at these experimental conditions.²⁸ This particular experiment achieved $\gamma = 17$. The BSE image highlights the types of mixing microstructures that develop with progressive shear strain, including the formation of monolayers, which are layers of recrystallized anhydrite that are a single grain thick. Black regions are decompression cracks that form after the experiment has concluded. (b) Experiment LVT_272 was conducted on a mixture of the minerals calcite and quartz. At the conditions of this experiment ($\gamma = 11$), syndeformational reactions produced the mineral wollastonite, which appears as the lightest color fringing the fractured quartz grains.

or grain size,²⁸ the viscosity contrast between constituent mineral phases,³⁹ and the volume proportions of the constituent mineral phases. Based on these experiments, the origins of (ultra)mylonites and their role in the formation of Earth-like plate boundaries are now better understood.

B. Recrystallization during deformation

Grain size evolves through a competition between static grain growth and dynamic recrystallization.^{42,43} Dynamic recrystallization can be further subdivided into a set of elemental microphysical

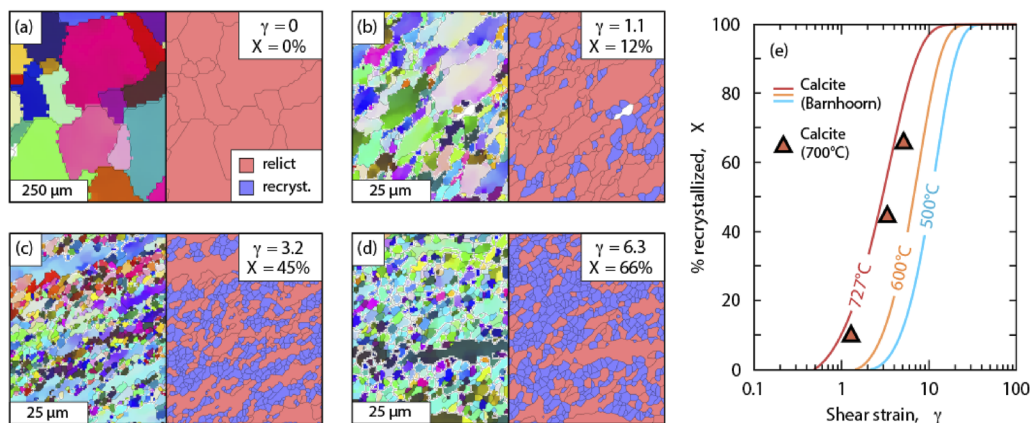


FIG. 6. Dynamic recrystallization in Carrara marble at high pressure and temperature, as a function of shear strain. (a)–(d) EBSD orientation maps (left) and maps showing the proportion of relict (red) vs recrystallized (blue) material (right) depict the evolution of microstructure at a given shear strain (γ). X is the area percentage of recrystallized grains. (e) The percentage of recrystallized grains (X) is plotted against shear strain, showing that a temperature-dependent, Avrami-type kinetic model fits the data well. A fit to the experimental data from Barnhoorn and co-authors⁴⁷ is included as solid curves for comparison.

processes, including sub-grain rotation, nucleation of strain-free grains, and (sub)grain boundary migration.⁴⁴ LVT experiments can help to unravel the complex dependencies of recrystallization processes on strain, temperature, and time.

In a previous study, we demonstrated that in a deforming crystalline solid, the percentage of recrystallized material increases with strain and is enhanced at greater homologous temperature (T/T_m , where T_m is the melting temperature).⁴⁵ Interestingly, this relationship is largely independent of material composition. We have further tested this relationship using benchmarking experiments in the LVT1 apparatus on Carrara marble ($T = 973$ K). In a series of experiments with different shear strains ($\gamma = 0, 1.1, 3.2, \text{ and } 6.3$), the area fraction of recrystallized material⁴⁶ was determined to increase monotonically according to the Avrami model⁴⁵ (Fig. 6). Furthermore, the data correlate remarkably well with measurements obtained by Barnhoorn and co-authors⁴⁷ using Paterson apparatus torsion experiments [Fig. 6(e), solid curves], demonstrating that the rate of dynamic recrystallization depends on temperature but is largely pressure-independent.

The LVTs are well-suited to further experiments of this type due to their large sample volume (which enables the use of coarse unrecrystallized starting materials) and ability to reach the shear strains necessary for complete recrystallization at low homologous temperatures ($T/T_m < 0.5$).

VIII. CONCLUSIONS

Experimental deformation provides a physical basis for interpreting geophysical data and parameterizing geodynamic models. High pressures and temperatures are necessary to ensure that experiments can be conducted in a fully viscous/plastic regime, without any unwanted artifacts from brittle fracture. Large specimen volumes are valuable because they permit the interrogation of microstructure over a range of length scales. The Large Volume Torsion (LVT) apparatus are uniquely capable devices that can achieve large strains, at high pressure and temperature, in relatively large specimens. The flexibility of the LVT press frame leaves open the option of adding new modules; for example, holders to deform granular materials. A limitation of the LVTs is that they do not yet provide precise measurements of rock strength due to the difficulty of measuring the torque applied to the specimen. Continued efforts to improve the LVT apparatus will seek to improve torque measurements through innovative approaches to force measurement.

ACKNOWLEDGMENTS

The authors gratefully thank all group members who conducted experiments and contributed to the development of the LVT apparatuses, including Katherine Billings, Maia Cohen, Emmett Ela, Timothy Howell, Charis Horn, Beno Jacob, Elizabeth Olree, and Jack Qidiao. The engineering teams at Enerpac and Milwaukee Cylinder are thanked for their input and assistance during the design process. Two reviewers are thanked for their constructive feedback on the manuscript. The LVT apparatuses were developed and acquired using grants from the NSF Instrumentation and Facilities program (Grant Nos. NSF EAR-1139706, EAR-1360584, EAR-1945763, and

EAR-2149427). The results described in Sec. VII were supported by Grant Nos. NSF EAR-1352306 and EAR-1853155. Partial support for electron microscopy is provided by the Institute of Materials and Engineering at Washington University in St. Louis.

AUTHOR DECLARATIONS

Conflict of Interest

The authors have no conflicts to disclose.

Author Contributions

Philip Skemer: Conceptualization (lead); Funding acquisition (lead); Methodology (equal); Supervision (lead); Writing – review & editing (lead). **Hélène Couvy:** Data curation (lead); Investigation (lead); Methodology (equal); Supervision (equal); Visualization (equal); Writing – original draft (equal). **Andrew J. Cross:** Investigation (equal); Methodology (supporting); Validation (equal); Writing – review & editing (supporting). **Joshua A.H. Littleton:** Data curation (supporting); Formal analysis (equal); Investigation (equal); Methodology (equal); Writing – review & editing (supporting). **Caroline Bollinger:** Investigation (supporting); Validation (supporting).

DATA AVAILABILITY

All data will be made available upon request to the corresponding author.

REFERENCES

- ¹G. F. Davies and M. A. Richards, “Mantle convection,” *J. Geol.* **100**(2), 151–206 (1992).
- ²Y. Ricard, “Physics of mantle convection,” *Treatise Geophys.* **7**, 23–71 (2015).
- ³V. S. Solomatov and L. Moresi, “Stagnant lid convection on Venus,” *J. Geophys. Res.: Planets* **101**(E2), 4737–4753, <https://doi.org/10.1029/95je03361> (1996).
- ⁴V. S. Solomatov and L. Moresi, “Three regimes of mantle convection with non-Newtonian viscosity and stagnant lid convection on the terrestrial planets,” *Geophys. Res. Lett.* **24**(15), 1907–1910, <https://doi.org/10.1029/97gl01682> (1997).
- ⁵W. F. Brace and D. L. Kohlstedt, “Limits on lithospheric stress imposed by laboratory experiments,” *J. Geophys. Res.* **85**(B11), 6248, <https://doi.org/10.1029/jb085ib11p06248> (1980).
- ⁶D. Yamazaki and S. Karato, “High-pressure rotational deformation apparatus to 15 GPa,” *Rev. Sci. Instrum.* **72**(11), 4207 (2001).
- ⁷K. F. Forsgren and H. G. Drickamer, “Design variables for a high pressure cell with supported taper pistons,” *Rev. Sci. Instrum.* **36**(12), 1709–1712 (1965).
- ⁸F. D. Adams, “An experimental investigation into the action of differential pressure on certain minerals and rocks, employing the process suggested by Professor Kick,” *J. Geol.* **18**(6), 489–525 (1910).
- ⁹F. D. Adams and J. T. Nicolson, “An experimental investigation into the flow of marble,” *Philos. Trans. R. Soc., A* **195**, 363–401 (1901).
- ¹⁰H.-R. Wenk, “Some roots of experimental rock deformation,” *Bull. Minéral.* **102**(2), 195–202 (1979).
- ¹¹T. E. Tullis and J. Tullis, *Experimental Rock Deformation Techniques* (American Geophysical Union, 1986).
- ¹²Y. Wang, W. B. Durham, I. C. Getting, and D. J. Weidner, “The deformation-DIA: A new apparatus for high temperature triaxial deformation to pressures up to 15 GPa,” *Rev. Sci. Instrum.* **74**(6), 3002–3011 (2003).
- ¹³D. Griggs, “Hydrolytic weakening of quartz and other silicates,” *Geophys. J. R. Astron. Soc.* **14**(1–4), 19 (1967).

- ¹⁴R. S. Borch and H. W. Green, "Deformation of peridotite at high pressure in a new molten salt cell: Comparison of traditional and homologous temperature treatments," *Phys. Earth Planet. Inter.* **55**(3–4), 269–276 (1989).
- ¹⁵C. W. Holyoke III and A. K. Kronenberg, "Accurate differential stress measurement using the molten salt cell and solid salt assemblies in the Griggs apparatus with applications to strength, piezometers and rheology," *Tectonophysics* **494**(1–2), 17–31 (2010).
- ¹⁶H. C. Heard, "Effect of large changes in strain rate in the experimental deformation of Yule marble," *J. Geol.* **71**(2), 162–195 (1963).
- ¹⁷M. S. Paterson, "A high-pressure, high-temperature apparatus for rock deformation," *Int. J. Rock Mech. Min. Sci. Geomech. Abstracts* **7**(5), 517–526 (1970).
- ¹⁸R. Heilbronner and J. Tullis, "Evolution of C axis pole figures and grain size during dynamic recrystallization: Results from experimentally sheared quartzite," *J. Geophys. Res.* **111**(B10), <https://doi.org/10.1029/2005jb004194> (2006).
- ¹⁹P. W. Bridgman, "Effects of high shearing stress combined with high hydrostatic pressure," *Phys. Rev.* **48**(10), 825–847 (1935).
- ²⁰M. S. Paterson and D. L. Olgaard, "Rock deformation tests to large shear strains in torsion," *J. Struct. Geol.* **22**(9), 1341–1358 (2000).
- ²¹M. T. L. Berg, G. D. Bromiley, I. B. Butler, M. Frost, R. Bradley, J. Carr, Y. Le Godec, L. G. J. Montési, W. Zhu, K. Miller, J. P. Perrillat, E. Mariani, D. Tatham, and S. A. T. Redfern, "Deformation-aided segregation of Fe-S liquid from olivine under deep Earth conditions: Implications for core formation in the early solar system," *Phys. Earth Planet. Inter.* **263**, 38 (2017).
- ²²G. D. Bromiley, S. A. T. Redfern, Y. Le Godec, G. Hamel, and S. Klotz, "A portable high-pressure stress cell based on the V7 Paris-Edinburgh apparatus," *High Pressure Res.* **29**(2), 306–316 (2009).
- ²³V. D. Blank, Y. S. Konyayev, A. I. Kuznetsov, and E. I. Estrin, "A diamond chamber for examining the effects of shear deformation on the structure and properties of solids at pressures up to 43 GPa," *Instrum. Exp. Tech.* **27**(5), 1240–1242 (1984).
- ²⁴Y. Ma, E. Selvi, V. I. Levitas, and J. Hashemi, "Effect of shear strain on the α - ϵ phase transition of iron: A new approach in the rotational diamond anvil cell," *J. Phys.: Condens. Matter* **18**(25), S1075 (2006).
- ²⁵R. Nomura, S. Azuma, K. Uesugi, Y. Nakashima, T. Irifune, T. Shinmei, S. Kakizawa, Y. Kojima, and H. Kadobayashi, "High-pressure rotational deformation apparatus to 135 GPa," *Rev. Sci. Instrum.* **88**(4) (2017).
- ²⁶K. K. Pandey and H. K. Poswal, "A new compact symmetric shear diamond anvil cell for in situ high-pressure-torsion studies," *Rev. Sci. Instrum.* **95** (2024).
- ²⁷C. W. Passchier and R. A. J. Trouw, *Microtectonics* (Springer-Verlag, 1998).
- ²⁸A. J. Cross and P. Skemer, "Ultramylonite generation via phase mixing in high-strain experiments," *J. Geophys. Res.: Solid Earth* **122**(3), 1744, <https://doi.org/10.1002/2016jb013801> (2017).
- ²⁹E. C. Lloyd, C. W. Beckett, and F. R. Boyd, "Measurements in the high-pressure environment," *Science* **164**(3881), 860–862 (1969).
- ³⁰G. Andersson, B. Sundqvist, and G. Bäckström, "A high-pressure cell for electrical resistance measurements at hydrostatic pressures up to 8 GPa: Results for Bi, Ba, Ni, and Si," *J. Appl. Phys.* **65**(10), 3943–3950 (1989).
- ³¹N. A. Dixon and W. B. Durham, "Measurement of activation volume for creep of dry olivine at upper-mantle conditions," *J. Geophys. Res.: Solid Earth* **123**(10), 8459–8473, <https://doi.org/10.1029/2018jb015853> (2018).
- ³²T. H. Bell and M. A. Etheridge, "Microstructure of mylonites and their descriptive terminology," *Lithos* **6**(4), 337–348 (1973).
- ³³S. H. White, S. E. Burrows, J. Carreras, N. D. Shaw, and F. J. Humphreys, "On mylonites in ductile shear zones," in *Shear Zo. Rocks.*, edited by J. Carreras, P. R. Cobbold, J. G. Ramsay and S. H. White, International ed. (Pergamon, Oxford, NY, 1980), pp. 175–187.
- ³⁴G. S. Lister and A. W. Snoke, "S-C mylonites," *J. Struct. Geol.* **6**(6), 617–638 (1984).
- ³⁵J. Linckens, M. Herwegh, and O. Muntener, "Linking temperature estimates and microstructures in deformed polymineralic mantle rocks," *Geochem., Geophys., Geosyst.* **12**, Q08004, <https://doi.org/10.1029/2011gc003536> (2011).
- ³⁶M. Herwegh, J. Linckens, A. Ebert, A. Berger, and S. H. Brodhag, "The role of second phases for controlling microstructural evolution in polymineralic rocks: A review," *J. Struct. Geol.* **33**(12), 1728–1750 (2011).
- ³⁷D. Bercovici and Y. Ricard, "Mechanisms for the generation of plate tectonics by two-phase grain-damage and pinning," *Phys. Earth Planet. Inter.* **202–203**, 27–55 (2012).
- ³⁸D. Bercovici and Y. Ricard, "Plate tectonics, damage and inheritance," *Nature* **508**(7497), 513–516 (2014).
- ³⁹A. J. Cross, E. Olree, H. Couvy, and P. Skemer, "How does viscosity contrast influence phase mixing and strain localization?," *J. Geophys. Res.: Solid Earth* **125**(8), 1–20, <https://doi.org/10.1029/2020jb020323> (2020).
- ⁴⁰C. M. Horn and P. Skemer, "Semi-brittle deformation of Talc at the base of the seismogenic zone," *Geophys. Res. Lett.* **50**(8), 1–9, <https://doi.org/10.1029/2022gl102385> (2023).
- ⁴¹K. Billings and P. Skemer, "Evolving microstructure during experimental deformation of Maryland diabase," *Earth Planet. Sci. Lett.* **627**, 118564 (2024).
- ⁴²J. H. P. de Bresser, H. J. H. Ter, and C. J. Spiers, "Grain size reduction by dynamic recrystallization; can it result in major rheological weakening?," in *Deformation Mechanisms, Rheology Microstructure*, edited by G. Dresen and M. Handy (Springer International, Berlin, Federal, Republic of Germany, 2001).
- ⁴³N. J. Austin and B. Evans, "Paleowattmeters: A scaling relation for dynamically recrystallized grain size," *Geology* **35**(4), 343 (2007).
- ⁴⁴J. L. Urai, W. D. Means, and G. S. Lister, "Dynamic recrystallization of minerals," in *Mineral and Rock Deformation - Laboratory Studies*, edited by B. E. Hobbs and H. C. Heard (American Geophysical Union, Washington, DC, 1986), Paterson Volume, pp. 161–199.
- ⁴⁵A. J. Cross and P. Skemer, "Rates of dynamic recrystallization in geologic materials," *J. Geophys. Res.: Solid Earth* **124**(2), 1324, <https://doi.org/10.1029/2018jb016201> (2019).
- ⁴⁶A. J. Cross, D. J. Prior, M. Stipp, and S. Kidder, "The recrystallized grain size piezometer for quartz: An EBSD-based calibration," *Geophys. Res. Lett.* **44**(13), 6667–6674, <https://doi.org/10.1002/2017gl073836> (2017).
- ⁴⁷A. Barnhoorn, M. Bystricky, L. Burlini, and K. Kunze, "The role of recrystallisation on the deformation behaviour of calcite rocks: Large strain torsion experiments on Carrara marble," *J. Struct. Geol.* **26**(5), 885–903 (2004).